JOURNAL OF MATERIALS SCIENCE 13 (1978) 1480–1486

The effect of microstructure and phase composition on the ionic conductivity of magnesium-doped sodium-beta-alumina

G. J. MAY
Chloride Silent Power Limited, Davy Road, Astmoor, Runcorn, Cheshire, UK

A. HOOPER
Materials Development Division, AERE Harwell, Oxfordshire, UK

The effect of seeding magnesium-doped sodium-beta-alumina with pure β''-alumina has been investigated; the resulting product has been compared with material with the same composition but unseeded. The manner in which this technique controls the microstructure and phase composition has been studied and related to the measured ionic conductivity.

1. Introduction

Fast ionic conduction in solids has become the subject of considerable research work in recent years [1, 2] and much of this activity has been concerned with sodium ion transport in sodium-beta-alumina because its application as the electrolyte and separator in sodium–sulphur cells has considerable commercial potential [3, 4]. The high ionic conductivity of beta-alumina results from its layered crystal structure which consists of layers of four close-packed planes of oxygen and aluminium ions in a spinel-like structure. These layers, referred to as spinel blocks, are separated by Al–O–Al pillars and Na^+ ions reside and migrate freely in an electric field in the loosely packed planes between the spinel blocks. There are two principal forms of beta-alumina; these are β-(hexagonal; $P6_3/mmc$; $a_0 = 0.559$ nm, $c_0 = 2.261$ nm) [5, 6] and β''- (rhombohedral; $R\bar{3}m$; $a_0 = 0.560$ nm, $c_0 = 3.395$ nm) [7, 8]. The two types differ essentially only in the stacking sequence of close-packed layers. β''-is rather more conductive than β-and is stabilized by small doping additions of Li and Mg which substitute for Al in the spinel blocks. The conduction plane readily undergoes cleavage but satisfactory mechanical strengths can be achieved in polycrystalline materials with uniform, fine-grained microstructures. This, however, reduces the overall ionic conductivity both because grain boundaries tend to have a higher ionic resistivity than the grain bulk and also, as compared to a single crystal, because the ions must follow a longer, tortuous path through the electrolyte membrane as they travel from one grain to the next. The optimum combination of microstructure and phase composition would be a uniform grain size in the range 25 to 50 μm in a material entirely converted to β''-alumina.

Microstructural control during sintering of beta-alumina is usually obtained by firing rapidly at a relatively high temperature for a short time. Under these conditions high sintered densities are achieved with very little grain growth (grain sizes are typically in the range 1 to 5 μm) but only partial conversion to β''-alumina takes place. Further conversion to β''-can be produced by heat treatment at a temperature less than the sintering temperature and little grain growth occurs until the temperature is raised to a threshold level at which runaway discontinuous grain growth occurs producing a mechanically weak material. It is, however, possible to produce beta-alumina with a larger, but uniform, grain size and virtually complete conversion to β''-by seeding the precursor powder with a small amount of pure β''-alumina made from finely-ground, sintered and heat-treated material. This technique has been studied for lithium-doped beta-alumina where pure β''-alumina with a grain size of 30 to 75 μm can be produced by seeding [9]. The ionic resistivity was $\sim 0.03\,\Omega$m at 575 K,

similar to extensively annealed material with a duplex microstructure of coarse grains in a fine grained matrix.

In this work, the effects of seeding with a small amount of pure β''-in a magnesium-doped beta-alumina have been investigated and the relative effects of the change in microstructure and phase composition have been studied. Polycrystalline material has been prepared and the ionic conductivity of seeded and unseeded material with the same composition has been measured by a.c. and d.c. techniques over a range of temperature (300 to 675 K) in order to separate the grain boundary and grain bulk components of the ionic resistivity.

2. Experimental

Beta-alumina samples were prepared in the form of thin-walled, closed-ended tubes, 33 mm outside diameter by 225 mm long with a wall thickness of 1.5 mm and as discs 10 mm in diameter by 5 mm thick. The two materials investigated, A and B, both had the composition 8 wt% Na_2O, 2 wt% MgO, 90 wt% Al_2O_3 but B had 10% of pure β''-alumina added as a seeding agent. The materials were made up from high purity starting materials in the form of finely ground α-alumina, magnesium oxide, sodium aluminate and in the case of B, pure β''-alumina. The seeding agent was prepared from the same starting materials but had a composition 9 wt% Na_2O, 4 wt% MgO, 87 wt% Al_2O_3. The powder was processed in the same manner as A and B, fabricated into tubes and sintered to produce a substantially coarse-grained microstructure. The tubes were then crushed and ground to a fine powder using a high amplitude vibratory mill. All the constituent oxides for both materials A and B were milled together in rubber-lined vibro-mills using α-alumina cylinders as grinding media to produce a homogeneous mixture. Green shapes were produced by isostatic pressing with a pressure of 275 MN m^{-2}. The samples were then fired in a rapid, pass-through zone sintering furnace with a peak temperature of 1975 K and a relatively short hot zone over a range of speeds from 40 to 60 mm min^{-1}. The furnace atmosphere was oxidizing and saturated with sodium oxide vapour. Sodium oxide loss by evaporation was effectively suppressed by this short, buffered firing cycle, as confirmed by X-ray fluorescence analysis of the sintered material

The proportions of the β- and β''-phases were estimated by measuring the relative peak heights of selected reflexions on an X-ray diffractometer trace. Lattice parameters for both phases were calculated with correctly indexed d-spacings using the Nelson–Taylor–Riley–Sinclair function to compensate for geometric errors. The microstructure was examined by optical microscopy after grinding with silicon carbide paper, polishing with 1 μm diamond paste and etching in H_3PO_4 at 675 K. Thin foils for transmission electron microscopy were prepared by grinding to a thickness of 10 to 15 μm and then ion-beam machining. The foils were examined in a Philips EM301 electron microscope operated at 80 kV.

Mechanical strength measurements were made by diametral compression of rings in an Instron testing machine with a cross-head speed of 0.5 mm min^{-1}. Loading at asperities was avoided by the use of thin, soft aluminium shims. The tensile fracture stress was calculated using the approximations of elasticity theory for thin walls and due allowance was made for any eccentricity in the tubes. Fracture surfaces were observed directly in an ISI TV Mini-SEM scanning electron microscope.

The ionic resistivity was measured both by a d.c. 4-probe method [10] and an a.c. 2-terminal method [11]. For the d.c. measurements, four silver wires were wrapped around the tube and each wire was wetted with a small amount of an aqueous solution of sodium nitrite and sodium nitrate in eutectic proportions. A small current was passed between the outer probes and the potential between the inner probes measured. Precautions were taken to eliminate errors resulting from electrode polarization, slight differences in the composition of the sodium nitrate/nitrite eutectic or slight compositional differences in the ceramic sample. The ionic resistivity was calculated from the measured resistance and the dimensions of the sample over a range of temperatures from 550 to 675 K. The a.c. measurements were made either on discs or sections cut from the tubes (10 mm × 10 mm × 1.5 mm) with vacuum-evaporated gold as electrodes. Electrical contact to the external circuit was made by platinum foils under spring pressure. Measurements were carried out in dry air at a pressure of ~30 N m^{-2} over a range of frequencies from 500 Hz to 2 MHz at temperatures between 300 and 675 K. The equipment consisted of Wayne Kerr bridges B221 (500 Hz to 20 kHz) and B601 (20 KHz to 2 MHz) used in conjunction with an external source (Krohn–Hite 4200) and detector (Marconi TF1100).

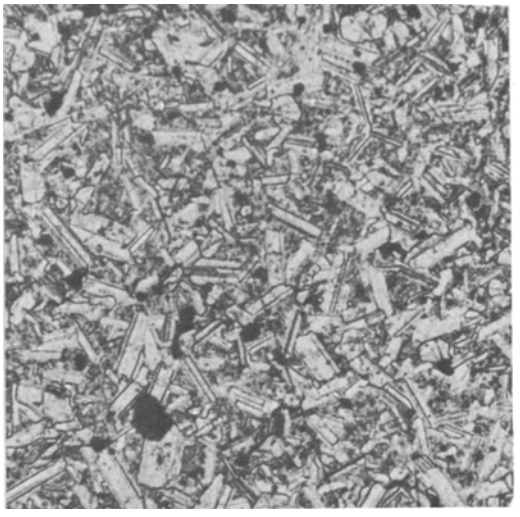

Figure 1 Microstructure of seeded magnesium-doped sodium-beta-alumina (B) showing porosity distribution and grains in a size range 20–60 μm many of which have distinct sub-boundaries, × 190.

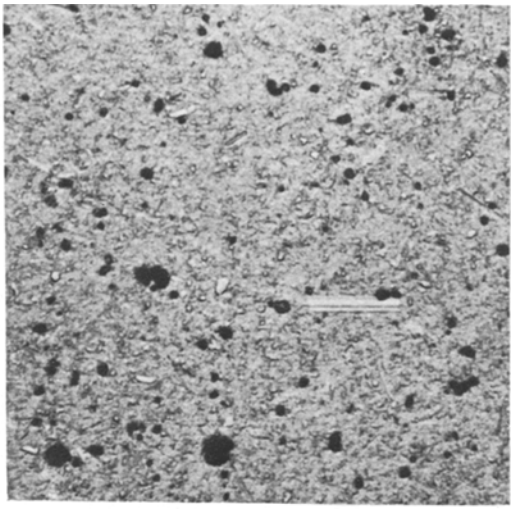

Figure 2 Microstructure of unseeded beta-alumina (A) showing porosity distribution and occasional large grains in a fine-grained matrix, × 270.

3. Results and discussion

3.1. Ceramic microstructure

The unseeded material (A) had a sintered density of 3240 kg m^{-3} (99% theoretical density) and the seeded material (B) a somewhat lower sintered density of 3210 kg m^{-3} (98% theoretical density) but both gave reliably impervious membranes in the form of tubes.

Both samples had a uniform pore-size distribution ranging from 1 to 20 μm in A and 2 to 30 μm in B. On etching, the microstructure of B was clearly revealed and consisted almost entirely of uniform grains in a size range of 20 to 60 μm with an average of 30 to 40 μm (Fig. 1). Many of the grains showed sub-boundaries and there were small areas of fine-grained material ($\sim$ 1 μm) between the larger grains. There was no evidence of discontinuous grain growth which is often a characteristic feature of sintered beta-alumina microstructures. The unseeded material (A) had a very fine-grained matrix (grain sizes in the range 0.5 to 2.0 μm) and a few larger lath-shaped grains ($<$1%) with a maximum length of 50 μm (Fig. 2). The fine-grained microstructure was resolved more clearly in the electron microscope (Fig. 3). The grain structure was uniform but there was a tendency for grains to be slightly elongated perpendicular to ⟨0001⟩. A substantial amount of sub-structure was visible in the ceramic grains. This has been characterized as dislocations in the basal plane [12], β/β'' intergrowth structures [13], complex faults normal to the basal plane [14], low-angle grain boundaries [15] and spinel intergrowths [16]. No intergranular second phases were apparent although a resolution limit of $\sim$ 10 nm must be set in the vicinity of grain boundaries; similarly no intragranular second phases larger than $\sim$2 nm were present. The β''-seeding material evidently provides a homogeneous distribution of nucleation sites for the growth of beta-alumina grains leading to competitive grain growth and a uniform microstructure. The small residual areas of fine-grained material indicate that the large grains grow in the fine-grained matrix at a fairly late stage of sintering. The slightly higher porosity suggests this occurs before sintering of the fine-grained material is complete as pores are trapped off in the large grains and close more sluggishly because of the larger pore–boundary distances. The size of the seeding material was important; the results described above were obtained with material ground to 5 to 10 μm before the final vibro-milling but finer beta-alumina seeding material with a particle size substantially all less than 1 μm failed to produce any microstructural control and the microstructure was similar to the unseeded material (A). It would appear that below a critical size the seeding agent is unstable on sintering and does not survive for a sufficient time to nucleate large grains.

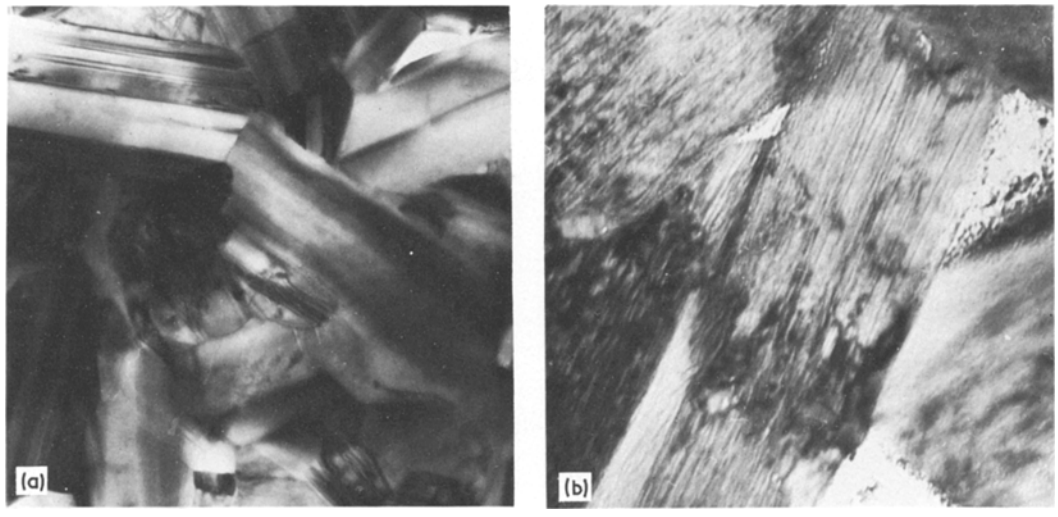

Figure 3 Transmission electron micrograph of beta-alumina (A) showing grain structure and sub-structure within the ceramic grains, (a) × 22 k, (b) × 90 k;

3.2. Phase composition and lattice parameters

The relative proportions of the β- and β''- phases were estimated from the heights of the $(01\bar{1}2)$, $(01\bar{1}3)$ β- and $(01\bar{1}2)$, $(10\bar{1}4)$ β''- peaks and from the $(02\bar{2}6)$, $(02\bar{2}7)$ β- and $(02\bar{2}10)$ β''- peaks. The volume fraction of β''- in the unseeded material (A) was ~0.50 whereas the volume fraction in the seeded material (B) was ~ 0.85. The volume fraction of β''- in the seeding agent itself (C) was >0.95 although small β-peaks were observed. The lattice constants and their standard deviations were evaluated from lattice parameters derived from individual d-spacings by a least squares analysis of these data, weighted to favour high angle lines, and using the Nelson–Riley–Taylor–Sinclair extrapolation function. The values are given in Table I.

The lattice parameters of the β-phase for B and C are inaccurate because of the low intensities and smaller number of peaks used. Comparing the values for the β''- phase shows no correspondence between the seeding agent itself and the seeded material and the β'' phase c_0 parameter for the unseeded material was different again. This indicates that there is no direct crystallographic relationship between the β''-phase in the various materials.

TABLE I

Material	Phase	a_0 (nm)	c_0 (nm)
A	β-	0.5609 ± 0.0004	2.235 ± 0.0002
A	β''-	0.5607 ± 0.0003	3.365 ± 0.005
B	β-	0.560 ± 0.002	2.27 ± 0.01
B	β''-	0.5607 ± 0.0002	3.378 ± 0.003
C	β-	0.557 ± 0.0003	2.28 ± 0.01
C	β''-	0.5623 ± 0.0005	3.365 ± 0.004

3.3. Mechanical strength

The change in grain size between the two materials was reflected in the mechanical strength with an average tensile strength of the unseeded material (A) of $250 \pm 25\,MN\,m^{-2}$ and of the seeded material (B) of $170 \pm 40\,MN\,m^{-2}$. This reduction is expected as a result of the increase in grain size but is, nonetheless, sufficient for use in an electrochemical cell. The fracture surface of material A was relatively featureless because of the fine scale of the microstructure (Fig. 4) and showed occa-

Figure 4 Fracture surface of fine-grained material (A). The grain structure is not apparent because of the fine grain size but some porosity is visible, SEM, × 1.25 k.

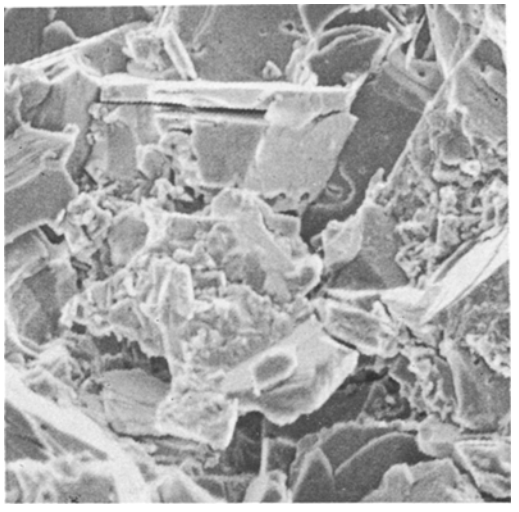

Figure 5 Fracture surface of coarse-grained material (B). Fracture has taken place by cleavage on the basal planes and some finer grained material is visible, SEM, × 1.25 k.

sional large grains that had fractured in a transgranular manner by cleavage. In contrast, the fracture surface of material B clearly showed intragranular fracture by cleavage on the basal plane (Fig. 5).

3.4. Ionic Conductivity

The overall electrical response r_t of a polycrystalline beta-alumina membrane is the sum of the grain bulk resistivity r_b and the grain boundary resistivity r_{gb} with an associated grain boundary capacitance C_{gb}. The equivalent circuit is shown in Fig. 6. Four terminal d.c. measurements give values of the overall resistivity but a.c. measurements allow the components of the circuit to be separated by the use of complex plane plotting. In the present experiments the real, G_p, and imaginary part, ωC_p, of the complex admittance are plotted. For the equivalent circuit assumed, the idealized complex admittance plot is shown in Fig. 6 and takes the form of two semi-circles which intersect with the real axis in two places to give both the overall resistivity and, at sufficiently high frequencies, the bulk resistivity. The form of the room temperature complex admittance plot typical for both types of specimen is also shown in Fig. 6. There were problems in that even at the highest frequency used (2 MHz) the whole of the second semi-circle was not resolved and in consequence only the value of the overall resistivity could be measured with precision. However, reasonable

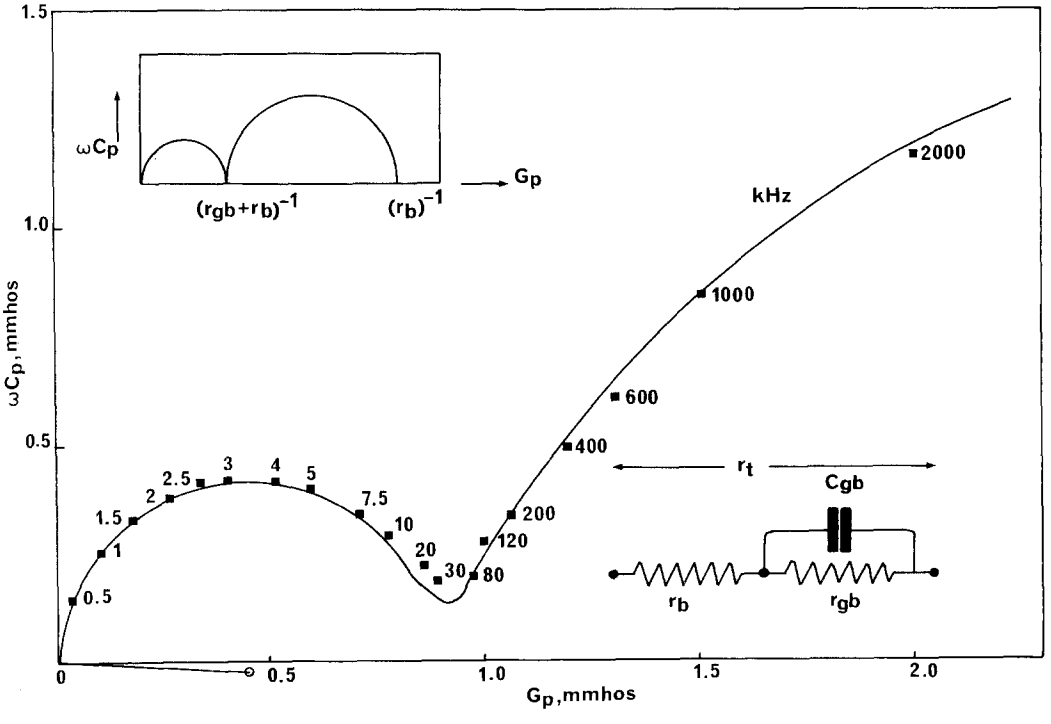

Figure 6 Complex plane plot of the real, G_p, and imaginary, ωC_p, parts of the admittance for seeded material (B) measured at 294 K over the range of frequencies shown. The insets show the form of equivalent circuit assumed and the ideal form of the complex plane plot for this equivalent circuit.

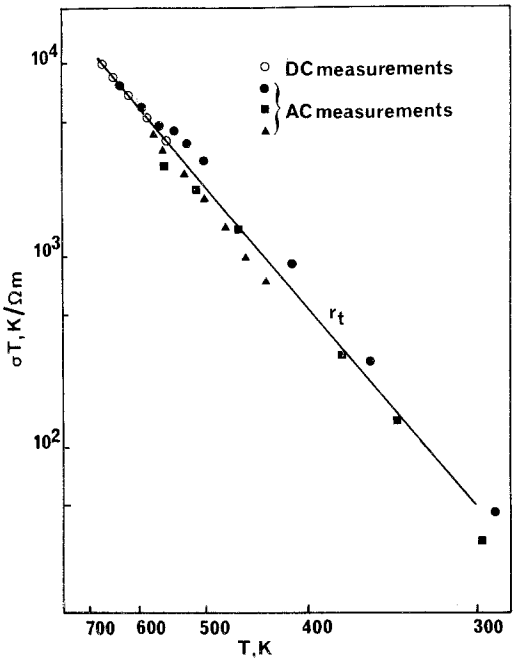

Figure 7 Arrhenius plot for unseeded material (A).

estimates of grain bulk resistivity were possible where a sufficient part of the high frequency semi-circle was observed. The inability to fully resolve the high frequency semi-circle is the result of a low value of C_{gb} which, in turn, can be inferred to result from a wide grain-boundary are plotted in Figs. 7 and 8 in the form of ln σT against reciprocal temperature and activation energies (E_a) are determined from the slopes of the straight line portions of the curves which obey an Arrhenius relation of the form $\sigma = (\sigma_0/T)\exp(E_a/RT)$ where σ_0 is a constant and R is the gas constant. The ionic resistivity determined from d.c. measurements on the unseeded material at 575 K was 0.122 Ωm, and the ionic resistivity of the seeded material at the same temperature was 0.053 Ωm. The corresponding activation energies were 23.2 kJ mol^{-1} and 14.3 kJ mol^{-1}. The ionic resistivity and activation energy of the highly doped seeding material were 0.040 Ωm (at 575 K) and 18.9 kJ mol^{-1}, respectively. The a.c. measurements of the seeded material allowed the bulk resistivity to be separated from the overall resistivity as shown in Figs. 6 and 8. The overall resistivity shows a change of slope at 550 K corresponding to a change in the activation energy from 21.2 kJ mol^{-1} at lower temperatures to the lower value determined by d.c. measurements at high temperatures. The bulk resistivity shows a single activation energy over the whole temperature range. We can conclude, therefore, that in this case grain-boundary effects only become dominant at temperatures close to ambient and the higher activation energy is associated with ionic transport across grain boundaries rather than in the bulk. The unseeded material on the other hand had no significant change of slope in the Arrhenius plot for the overall resistivity. There was agreement between the four-terminal d.c. measurements and two-terminal a.c. measurements and also with two-terminal a.c. measurements carried out independently with the same material [16]. It was not possible to separate the grain bulk resistivity from the overall resistivity but the high activation energy indicates that the grain-boundary contribution is dominent and extends at least up to 675 K. The extension of the grain-boundary-dominated region in the unseeded material to higher temperatures is consistent with the smaller grain size of this material as this results in an increased grain-boundary volume. The possibility that the observed improvement in conductivity of the seeded over unseeded material may be ascribed to the introduction of some electronic contribution to the conductivity may be readily discounted both from the form of the complex plane plots and also because both materials show full open-circuit voltages in sodium–sulphur cells.

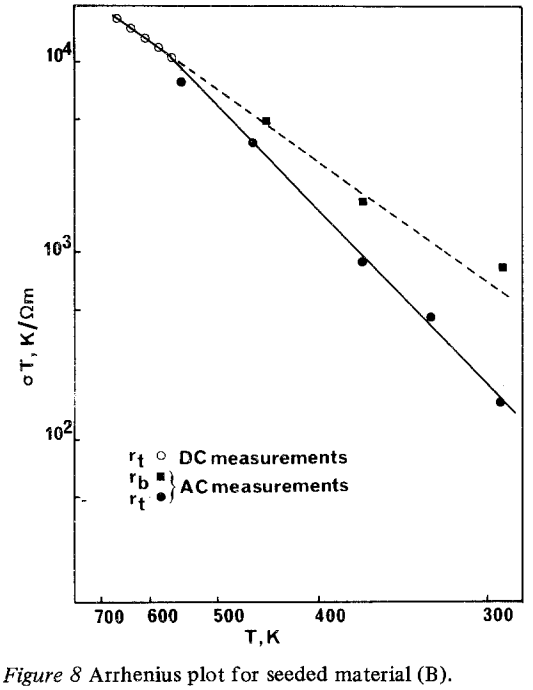

Figure 8 Arrhenius plot for seeded material (B).

The values determined for the different components of the ionic resistivity may be compared with the ionic resistivity of single crystal samples

of undoped β-alumina [2, 17, 18] and magnesium doped β″-alumina [2]. The ionic resistivity of β-alumina is ~0.30 Ωm at 295 K and ~0.05 Ωm at 575 K with an activation energy of ~13 kJ mol^{-1}. The ionic resistivity of β″-alumina is ~0.12 Ωm at 295 K and ~0.01 Ωm at 575 K with an activation energy of ~14 kJ mol^{-1}. The experimentally determined activation energy for the grain bulk component of the seeded material is similar to the single crystal value and whilst at first sight the resistivity values do not appear to agree with the relative volume fraction of the two phases, it must be remembered that there is also a tortuosity factor to be taken into account in the case of a polycrystalline specimen.

It is of interest to calculate the approximate resistance per unit area of grain boundary in these specimens. At 295 K the overall resistivity of the seeded material was 1.8 Ωm, the grain-boundary component being 1.4 Ωm and the grain bulk component, 0.4 Ωm. The median grain size of this material was 35 μm which corresponds to a grain-boundary area per unit volume of ~80 mm^2 mm^{-3} and thus a resistance per unit area of boundary of ~18 Ω mm^{-2}. Using this value the grain boundary component of a material with a grain size of 1.5 μm (grain boundary area/unit volume ~2000 mm^2 mm^{-3}) would be ~36 Ωm but the experimentally measured value for material A was 5.2 Ωm. The grain-boundary regions are therefore evidently dissimilar in the two materials.

4. Conclusions

Polycrystalline magnesium-doped beta-alumina tubes and discs have been prepared by a seeding technique in which 10% of pure β″-alumina seeding material has been used to produce a uniform microstructure with a grain size in the range 15 to 75 μm and a substantial proportion of β″-alumina (~85%) without heat treatment subsequent to sintering. The properties of this material have been measured and compared with an unseeded material having the same composition but a fine-grained microstructure in the range 0.5 to 2.0 μm and a smaller proportion of β″-alumina (~50%). The ionic resistivity of the seeded material was substantially lower than that of the unseeded material being 0.053 Ωm as compared to 0.12 Ωm at 575 K and the relative contribution of the grain boundary and grain bulk components were consistent with the grain size and phase composition of the two materials. The mechanical strength has been shown to be adequate for use in sodium–sulphur cells. The seeding procedure is useful for the preparation of highly conductive electrolyte tubes for use in sodium–sulphur cells without the need for post-sintering anneal and with a high degree of microstructural control. It also allows conductive materials to be prepared in beta-alumina compositions in which a high volume fractions of β″- cannot be produced by a conventional sintering/heat-treatment route.

Acknowledgements

The assistance of Stephen Tan, Allan Gibson and Sheila Ruddlesden with this work and the permission of Chloride Silent Power Limited to publish this paper are gratefully acknowledged.

References

1. P. McGEEHIN and A. HOOPER, *J. Mater. Sci.* **12** (1977) 1.
2. J. T. KUMMER, *Prog Solid State Chem.* 7 (1972) 141.
3. N. WEBER and J. T. KUMMER, *Adv. Energy Conv. Eng.* ASME Conference, Florida (1967) p.913.
4. G. J. MAY and I. W. JONES, *Metall. Mater. Techn.* 8 (1976) 427.
5. W. L. BRAGG, C. GOTTFREID and J. WEST *Z. Krist.* 77 (1931) 255.
6. C. A. BEEVERS and M.A.S.ROSS, *ibid* 97 (1937) 59.
7. Y. YAMAGUCHI and K. SUZUKI, *Bull. Chem. Soc. Japan* **41** (1968) 93.
8. M. BETTMAN and C. R. PETERS, *J. Phys. Chem.* 73 (1969) 1774.
9. S. A. WEINER and R. P. TISCHER, "Research on Electrodes and Electrolyte for the Ford Sodium–Sulphur Battery," Report on Contract No.: NSF–C805 (AER-73-07199) July 1976.
10. L. J. MILES and I. W. JONES, *Proc. Brit. Ceram. Soc.* **19** (1969) 161.
11. A. HOOPER, *J. Phys. D : Appl. Phys.* **10** (1977) 1487.
12. R. STEVENS, *J. Mater. Sci.* 9 (1974) 801.
13. J. M. BEVAN, B. HUDSON and P. T. MOSELEY, *Mat. Res. Bull.* 9 (1974)1073.
14. L. C. De JONGHE, *J. Mater. Sci.* **10** (1974) 2173.
15. L. C. De JONGHE and M. Y. HSIEH, Proc. Symp. and Workshop on Advanced Battery Research, March 1976, Argonne National Laboratory, B13.
16. L. C. DeJONGHE, personal communication (February, 1977).
17. W. L. FIELDER, H. E. KAUTZ, J. S. FORDYCE and J. SINGER, *J. Electrochem. Soc.* **122** (1975) 528.
18. R. D. ARMSTRONG, T. DICKINSON and P. M. WILLIS, *J. Electroanal. Chem.* 67 (1976) 121.

Received 31 August and accepted 7 November 1977.